Manganese hydrides and superhydrides at high pressure

Jean-Baptiste Charraud,* Grégory Geneste,† and Marc Torrent
CEA, DAM, DIF, F-91297 Arpajon, France

(Received 17 June 2019; revised manuscript received 21 October 2019; published 3 December 2019)

Manganese hydrides and superhydrides have been studied from ambient up to high pressures by the *ab initio* random structure searching algorithm. At ambient pressure conditions and room temperature, the subhydride Mn_2H (space group $P\bar{3}m1$) is the only compound found stable among those studied, since ϵ-MnH (hcp structure, space group $P6_3/mmc$), although stable at 0 K, is destabilized by thermal effects. With increasing pressure, MnH is stabilized, and then hydrogen-rich hydrides appear: first MnH_2 around 30 GPa, then MnH_7 around 40 GPa, and finally MnH_3 around 90 GPa. MnH_8 is likely to become stable around 150 GPa. The body-centered tetragonal structure of MnH_2 (space group $I4/mmm$) is identical to that of FeH_2 and CoH_2. MnH_3 has an original body-centered tetragonal structure, with space group $I4/m$ and 4 formula units per primitive cell. It contains a structural unit H_8 with rather short H-H distances. MnH_7 is extremely stable at high pressure. MnH_7 and MnH_8 exhibit a mixed structure, with one hydrogen being under the molecular form ($1/2$ H_2) and the other ones under an atomic (hydrided) form. Atomic charges computed by the Bader method confirm the electron transfer from Mn to H, with Mn oxidation increasing from MnH to MnH_3, and then saturating beyond. At high pressure, nuclear quantum effects tend to stabilize MnH_4 and increase the stability of MnH_8.

DOI: 10.1103/PhysRevB.100.224102

I. INTRODUCTION

Superhydrides are newly discovered materials characterized by a large hydrogen content in their chemical formula (e.g., FeH_5 [1], LaH_{10} [2], and CeH_9 [3]), typically larger than what may be expected from usual valence rules, that apply at ambient pressure. These intriguing compounds, made of metal atoms combined with atomic hydrogen around them, are stabilized by high-pressure conditions and are currently the subject of intensive research because of their very promising potentialities. Indeed, if superhydrides could survive at ambient pressure under a metastable form, they could be used as efficient solid-state hydrogen storage systems, provided their formation energy remains sufficiently negative. Furthermore, it can be noted that hydrogen solubility in the metal usually increases with pressure, which suggests that very hydrogen-rich compounds may be formed at sufficiently large synthesis pressures. In this respect, the series of iron hydrides, FeH_x, is emblematic: iron and hydrogen form FeH under a few GPa [1,4–8], and then successively FeH_2 at 67 GPa [5], FeH_3 at 87 GPa [5], and FeH_5 at ∼130 GPa [1].

Another challenge with high-pressure hydrides is the possible obtention of conventional superconductors with high critical temperature (T_c). This is guided by Ashcroft's idea [9], according to which the high-T_c superconductivity expected in metallic hydrogen at large pressure (pure hydrogen is expected to metallize around 450 GPa [10]) could be encountered also in some metal-hydrogen alloys, but at more moderate pressure, due to a chemical precompression of the hydrogen lattice by the metal atoms. After the discovery of high-T_c superconductivity in H_3S in the 150–200 GPa range [11], several hydrides and superhydrides have been predicted as superconductors under pressure. The rare-earth hydrides, and the hydrides of transition metals belonging to column IIIB of the periodic table (Sc, Y, La), have been predicted so far with the highest T_c: yttrium superhydrides [12–14], for instance YH_6 and YH_{10}, exhibit predicted superconducting T_c around 250–280 K [15]. They should also reach very high hydrogen stoichiometries, typically RH_6, RH_9, or RH_{10} (R = rare earth or IIIB transition metal). Very recently, these predictions seem to have received experimental confirmation in the case of lanthanum decahydride, LaH_{10} [16,17]. Note that these compounds RH_x adopt at large x ($\gtrsim$5–6) very specific crystal structures with the hydrogen atoms arranged in cages that surround the metal atoms ("hydrogen clathrate structures" [14]). Also, actinides such as U [18], Ac [19], and Th [20] have been shown to form superhydrides under pressure, some of them possibly exhibiting interesting superconducting properties.

Superhydrides have also been observed and predicted in the family of transition metals [21]: iron pentahydride, FeH_5, is formed at 130 GPa [1], while CrH_8 is predicted to appear at 132 GPa [22]. Other transition metals, in contrast, are not observed or predicted to form hydrides MH_x beyond $x = 3$. Cobalt, for instance, is predicted to form hydrides up to CoH_3 [23], with CoH and CoH_2 being observed [24]. Nickel is predicted to form hydrides up to NiH_2 at 60 GPa [25], with Ni_2H_3 being observed [25,26] in this pressure range. Note that mono-, sesqui-, and dihydrides of transition metals often adopt an already reported crystal structure. Monohydrides MH, for instance, adopt in most cases, either an hcp arrangement (ϵ phase), a rocksalt structure (γ phase), or a double hcp structure (ϵ' phase). Table S1 in the Supplemental Material [27] summarizes the observed or predicted structures of the

*jean-baptiste.charraud@cea.fr
†gregory.geneste@cea.fr

MH_x, with M a $3d$ transition metal [1,5,6,22,24–26,28–31] (with the exception of Sc because Sc hydrides [32] are closer to the family of rare-earth hydrides). In this work, we focus on manganese, a $3d$ transition metal for which the high-pressure hydriding properties have been investigated only up to 30 GPa, to the best of our knowledge [33]. Mn lies next to Fe in the periodic table and is less electronegative than Fe (Mn is 1.55, Fe is 1.83, H is 2.2 on the Pauling scale of electronegativities [34,35]), suggesting a larger electron transfer to hydrogen in Mn hydrides than in Fe hydrides. Since Fe has the capability to form hydrogen-rich compounds under high pressure, in which hydrogen is completely hydrided (i.e., not under a molecular form), at least up to FeH_5 [1], it is suggested that Mn could also form hydrogen-rich compounds, possibly superhydrides in similar conditions.

At ambient pressure and up to ∼710°C [36], Mn adopts a complex cubic-type structure, called α-Mn (space group $I\bar{4}3m$, 58 atoms per conventional cell) [37,38]. Three other allotropic phases are reported with increasing temperature: the β phase (also a complex cubic-type structure), the γ (fcc) phase, and then the δ (bcc) phase [36]. Manganese hydrides were investigated in past years at low and moderate pressures up to 30 GPa [33]. It was demonstrated that under pressure, hydrogen may be inserted into manganese, forming three types of hydrides MnH_x: (i) ϵ hydrides [33,36,39–44], having a H-to-metal ratio x between 0.65 and 0.96 under pressure [42,44], in which the H atoms randomly occupy the interstitial octahedral sites of an hcp lattice of manganese; (ii) γ hydrides, with a H-to-metal ratio x between 0 and 0.5 [45] (the γ phase is reported up to $x = 0.64$ [33]) in which the H atoms randomly fill the interstitial octahedral sites of an fcc Mn lattice; and (iii) for very small H-to-metal ratio $x \leqslant 0.1$, solid solutions of hydrogen in α- and β-Mn are also reported [36]. At moderate temperature and under pressure, formation of ϵ-MnH_x seems to be favored [36], while γ-MnH_x requires high temperature (e.g., above 900°C under 1.2 GPa according to Ref. [46], and above 325°C according to Ref. [47]). Once formed, the hcp structure of ϵ-MnH_x ($x = 0.84$) is maintained at least up to 30 GPa, while γ-$MnH_{0.64}$ undergoes an irreversible transformation into the hcp phase with pressure [33]. This transformation from γ to ϵ was already reported by Filipek *et al.* [48]. Therefore, the γ-MnH_x hydrides are stable at high temperature, while the ϵ-MnH_x hydrides are stable at low temperature [44]. A double hcp phase (ϵ'-MnH_x) was also reported under pressure and at high temperature (∼800°C) [49]. Very recently, in another context, manganese hydrides have been synthesized under a molecular form and used to build an efficient hydrogen storage system [50].

The aim of the present work is to extend the knowledge of the manganese hydrides to the pressure regime currently and easily accessible to diamond anvil cells, i.e., to ∼150 GPa, and to predict whether new forms of hydrided manganese, e.g., superhydrides, may be stable under high pressure. We show that Mn forms mono-, di-, and trihydrides under pressure, and we find a very stable Mn superhydride MnH_7, stable at moderate pressure of ∼44 GPa. Hydrogen in this manganese heptahydride MnH_7 is partly molecular, as in MnH_8 (which is likely to appear beyond 150 GPa). MnH_4 and MnH_8 are stabilized at high pressure by nuclear quantum effects.

II. COMPUTATIONAL DETAILS

A. *Ab initio* random structure searching

Our structural searches on the manganese hydrides are performed in the framework of the *ab initio* random structure searching (AIRSS) algorithm, as introduced by Pickard and Needs [51]. The stoichiometries here considered are MnH_x, with x varying from 1 to 8, with 1, 2, 3, and 4 formula units (f.u.) per simulation cell. Also, we have explored the possibility of half-integer hydrogen stoichiometries, Mn_2H_{2x}, with x being a half integer from 0.5 to 7.5, using unit cells with 1 and 2 f.u.

For each considered stoichiometry and number of formula units, a set of initial atomic configurations is randomly generated and then structurally optimized by density-functional theory (DFT). The random generation concerns atomic positions, lattice constants, and cell angles. The volume distribution of these initial cells is around a reference volume (that depends on the number of formula units and hydrogen stoichiometry), chosen close to that already known of the iron hydrides (which can be justified by remarking that the ionic radius of Mn is close to that of Fe). Mainly for practical reasons, a bias on initial interatomic distances is enforced in the random generation, to avoid initial configurations having unphysically short bond lengths. The number of structural optimizations performed for each considered stoichiometry and number of formula units is typically a few hundred, varying from ∼100 up to more than 1000. These structural optimizations are performed using the Broyden-Fletcher-Goldfarb-Shanno (BFGS) algorithm and consist of an optimization of both atomic positions and cell vectors to match a chosen hydrostatic pressure. Searches have been done for pressures of (i) 50 GPa for MnH_x with x from 1 to 3, and Mn_2H_{2x} with x a half integer from 0.5 to 7.5; (ii) 100 GPa for MnH_x with x from 1 to 8, and Mn_2H_{2x} with x an half integer from 4.5 to 7.5; and (iii) 150 GPa for MnH_x with x from 2 to 8. The results presented here can therefore be considered predictive for pressures up to 150 GPa.

At the end of each structural optimization, the final enthalpy is computed, which allows identifying the most stable structure by comparing all the enthalpies obtained for a given hydrogen stoichiometry. In practice, we have also examined the structures having a slightly higher enthalpy (typically 50 meV/atom). In most cases, the most stable structure appears several times along the AIRSS procedure.

The space group and Wyckoff positions of the selected structures are determined using the FINDSYM program [52,53]. For the random generation, we have used the nondeterministic random number generator of Chandler and Northrup [54].

B. Density-functional theory calculations

Our DFT calculations are performed with the ABINIT code [55], within the projector-augmented wave (PAW) formalism [56,57]. The exchange-correlation energy functional is the generalized gradient approximation as formulated by Perdew, Burke, and Ernzerhof [58] (GGA-PBE) throughout this work. We take the PAW atomic data sets for Mn and H from the Jollet-Torrent-Holzwarth table [59].

The structural optimizations at the AIRSS stage are performed using the BFGS algorithm as implemented in ABINIT. They use a $6 \times 6 \times 6$ k-point mesh (and $4 \times 4 \times 4$ for the largest cells) to sample the Brillouin zone associated with the simulation cell. A plane-wave cutoff of 15 or 20 hartrees is employed. The optimization criterion on atomic forces is 2×10^{-3} hartree/bohr (and 2×10^{-5} hartree/bohr^3 on stress tensor components). The AIRSS structural optimizations are also limited to at least 75 ionic steps.

Then, the structures identified as candidates for the MnH_x compounds are reoptimized using the BFGS algorithm, at several pressures between 0.0005 hartree/bohr^3 ($\sim$14.7 GPa) and 0.005 hartree/bohr^3 ($\sim$147 GPa), using more stringent numerical parameters: a plane-wave cutoff of 30 hartrees, a $12 \times 12 \times 12$ k-point mesh to sample the Brillouin zone associated with the simulation cell, and an optimization criterion on atomic forces of 1.0×10^{-6} hartree/bohr (and 1×10^{-8} hartree/bohr^3 on stress tensor components).

Dense hydrogen in the pressure range studied here (phases I and II) is subject to very large quantum fluctuations [60,61], with the dihydrogen molecules rotating and having no well-defined orientation. However, we use here as reference for solid hydrogen the $C2/c$-32 [61–63] (below 117 GPa) and $C2/c$-24 [64] phases (above 117 GPa) [27].

The dynamical stability of the predicted crystal structures for the manganese hydrides was then tested by computing at several pressures the phonon dispersion curves. These calculations have been performed within the framework of the density-functional perturbation theory (DFPT), as implemented in ABINIT [65,66], for MnH (at 50 and 150 GPa), MnH_2 (at 50, 100, and 150 GPa), MnH_3 (at 150 GPa), and MnH_7 (at 150 GPa). For these calculations, the structure was first fully reoptimized (criterion on atomic forces of 1.0×10^{-6} to 1.0×10^{-5} hartree/bohr). The meshes used in these DFPT calculations to sample the Brillouin zone for the electronic DFPT calculation and for the phonon grid are given in Ref. [27]. At 150 GPa, we have included the contribution of phonon zero-point energies (ZPEs) to the formation enthalpies of the hydrides, which implied phonon DFPT calculations also for several energetically unstable compounds (only the closest to the convex hull were tested, i.e., MnH_4, Mn_2H_9, MnH_5, Mn_2H_{11}, Mn_2H_{13}, and MnH_8) and for solid molecular hydrogen in phase $C2/c$-24 [64].

III. MANGANESE HYDRIDES AT AMBIENT AND LOW PRESSURE

A. Manganese hydrides at ambient pressure

As reported in the Introduction, manganese hydrides, MnH_x, have been synthesized in previous experimental studies up to $x = 0.84$ [33]: the structure of this MnH_x was shown to be hexagonal closed-packed (ϵ phase, hcp, space group $P6_3/mmc$). Our AIRSS results for MnH are in agreement with this result, since the hcp structure frequently appears in our search and is found as the most stable. Since MnH has been also synthesized (at high temperature) in the rocksalt structure (γ-MnH, space group $Fm\bar{3}m$), we have checked that this γ phase is less stable than the ϵ phase (this was tested up to $\sim$150 GPa). Also, the double hcp (dhcp) phase (ϵ'), which is the low-temperature structure of FeH [67], is found less stable than the ϵ phase. Note that the enthalpies of these three phases obey the order $\epsilon < \epsilon' < \gamma$ (see Ref. [27], Fig. S1), which is coherent with the experimental phase diagram proposed in Ref. [49], where the dhcp phase has been observed at temperatures intermediate between those of ϵ and γ. Note that our AIRSS results also revealed a structure with the $R\bar{3}m$ space group having an enthalpy intermediate between that of ϵ and that of ϵ' (r-MnH, see Ref. [27], Figs. S1 and S2). The structure of ϵ-MnH is the same as that of CrH [22,28].

In order to characterize the Mn hydriding process under ambient pressure conditions, we also consider Mn_2H and Mn_2H_3, in the structures determined by our searches. Mn_2H is found to crystallize in space group $P\bar{3}m1$ (as Cu_2H [29]), and its structure can be described as that of an interstitial hydride, with the H atoms partly filling the interstitial octahedral sites of a Mn hcp lattice (see Sec. V A). Mn_2H_3 is found to crystallize in space group $C2/m$, as Cr_2H_3 at low pressure [22] (see Ref. [27], Fig. S3).

For pure Mn at zero pressure, we did not perform any structural search. We consider here the α phase, which is the observed phase of Mn at ambient pressure and room temperature: it has a complex cubic structure with 58 atoms per conventional cell. Note that α-Mn is known as a complex noncollinear antiferromagnet below its Néel temperature of 95 K [38]. Reproducing these complex magnetic properties is beyond the scope of this work; thus we ignored the magnetism in α-Mn. First, we compute the formation enthalpies ΔH_f of Mn_2H, MnH, and Mn_2H_3 at zero pressure, which are the energies of the following processes:

$$\mathrm{Mn}(s) + \frac{x}{2}\mathrm{H_2}(g) \rightarrow \frac{1}{2}\mathrm{Mn_2H_{2x}}(s) \qquad (1)$$

with $x = 0.5$, 1, or 1.5, with all the solids optimized at zero pressure, and H_2 modeled as a single molecule in a large simulation box. We obtain $\Delta H_f(\mathrm{Mn_2H}) = -0.094$, $\Delta H_f(\mathrm{MnH}) = -0.135$, and $\Delta H_f(\mathrm{Mn_2H_3}) = +0.103$ eV/Mn. The negative hydriding enthalpy obtained for Mn_2H and MnH suggests that these two compounds may be formed spontaneously in ambient pressure conditions and 0 K. Mn_2H_3, in contrast, cannot be formed in such conditions. However, at finite temperature, it is necessary to consider the *free enthalpies* of formation of the hydrides, ΔG_f, which take into account thermal energetic and entropic effects. We compute an approximation of ΔG_f by adding to the total energy of the H_2 molecule the supplement of chemical potential, $2\Delta\mu_H$, as obtained assuming ideal gas behavior [68–70]. We assume the hydrogen gas pressure to be $P_{\mathrm{H_2}} = 1$ bar, and perform two numerical applications, for $T = 300$ and 600 K (Table I). This corresponds to $\Delta\mu_H = -0.159$ and -0.380 eV, respectively. Thermal (mainly entropic) effects stabilize the gas. At 300 K, this results in a negative formation free enthalpy for Mn_2H, but positive for MnH, while at 600 K, all the free enthalpies are positive. This suggests that under $P_{\mathrm{H_2}} = 1$ bar and at room temperature, MnH is not stable, and only subhydrides with less hydrogen (such as Mn_2H) are able to form.

Note that at ambient pressure and room temperature, MnH and Mn_2H_3 have a positive formation free enthalpy, which probably makes them rather unsuitable as efficient hydrogen storage systems (for which one rather expects both

TABLE I. Formation free enthalpies ΔG_f (eV/Mn) of Mn_2H, MnH, and Mn_2H_3 at ambient pressure and different temperatures. The chemical potential of the hydrogen gas is calculated assuming a hydrogen pressure $P_{H_2} = 1$ bar.

Compound	$T = 0$ K	$T = 300$ K	$T = 600$ K
Mn_2H	−0.094	−0.014	+0.096
MnH	−0.135	+0.024	+0.245
Mn_2H_3	+0.103	+0.342	+0.673

dynamical stability and a negative enough formation energy). The hydrides coming next in the series, and which are presented in the next sections, also have very positive formation free enthalpies at ambient pressure and room temperature, e.g., $\Delta G_f(MnH_2) = +0.63$ eV/Mn.

B. Manganese hydrides at low pressure

We now consider the hydriding process of Mn at ∼14.7 GPa (0.0005 hartree/bohr^3). At such pressure, we still use the α phase of Mn as a reference for the computation of the formation enthalpies, and take for hydrogen the $C2/c$-32 phase (see Ref. [27], Table S3). The formation enthalpies of the Mn hydrides found by our structural searches are plotted in Fig. 1. At such pressure, only Mn_2H and ϵ-MnH lie on the convex hull, suggesting that only hydrides MnH_x, with $x \leqslant 1$, can be formed, adopting interstitial structures with the H atoms filling the interstitial octahedral sites of an hcp lattice of Mn. We have already noticed that manganese hydride has been synthesized under pressures up to 30 GPa: the hydride observed was ϵ-MnH_x (hcp structure), with $x = 0.84$ [33]. Under pressure, the H-to-metal ratio in ϵ-MnH_x is reported to be lower than 1 [42,44]. This experimental result (i.e., only interstitial MnH_x compounds with $x \leqslant 1$ can be formed under low- and moderate-pressure conditions) is thus coherent with the present work.

Note that experimental studies report the observation of disordered solutions, i.e., the H atoms are randomly distributed over the octahedral interstitial sites of the hcp lattice, at least for $x \geqslant 0.83$ [44]. This configurational disorder may be a cause of stabilization because of the associated configurational entropy. Such disordered states are obviously not accessible by our AIRSS.

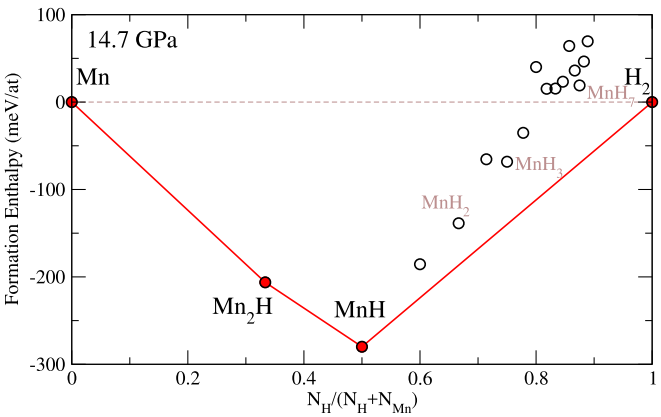

FIG. 1. Formation enthalpies (meV/atom) of Mn hydrides at 14.7 GPa. The α phase of Mn is taken as a reference. Phonon ZPEs are not included.

At smaller H-to-metal ratio, however, e.g., for $x = 0.65$, the H atoms in ϵ-MnH_x have been observed to presumably locate in one particular family of octahedral sites, namely, within one (0001) plane among two. This was reported in Refs. [44,71,72]: the H atoms can be viewed as forming a superstructure within the sublattice of the octahedral sites, of the anti-CdI_2 type (space group $P\bar{3}m1$; the (0001) planes of octahedral sites filled with H alternate along the hcp axis). This exactly corresponds to the structure found in our AIRSS for Mn_2H (see Sec. V A).

IV. MANGANESE HYDRIDES AND SUPERHYDRIDES AT HIGH PRESSURE

We now turn to the description of hydrides and superhydrides that appear at high pressures, typically up to 150 GPa. The α phase of Mn is known to be stable up to 165 GPa [37]. However, we consider here the formation enthalpies of the hydrides with respect to ϵ-MnH (rather than α-Mn) and solid hydrogen, in order to make more visible the region with the large hydrogen stoichiometries. The formation enthalpy $\Delta H_f^{\mathrm{MnH}}(MnH_x)$ with respect to MnH and H_2 is thus the enthalpy of the process

$$\mathrm{MnH}(s) + \frac{x-1}{2}\mathrm{H_2}(s) \rightarrow \mathrm{MnH}_x(s). \qquad (2)$$

For a hydride MnH_x, we denote by N_{MnH} the number of MnH groups in the formula unit MnH_x, and by N_{H} the number of remaining H atoms (once MnH has been removed), i.e., $N_{\mathrm{MnH}} = 1$ and $N_{\mathrm{H}} = x - 1$. In order to keep a correct meaning regarding their convex hull, these enthalpies (per formula unit), if plotted as a function of hydrogen content $N_{\mathrm{H}}/(N_{\mathrm{MnH}} + N_{\mathrm{H}})$, must be divided by $N_{\mathrm{MnH}} + N_{\mathrm{H}}$ ($= x$ in the present case), and not by the number of atoms. This is done in Fig. 2 for pressures of 29, 44, 58, 88, 117, and 147 GPa, and in Sec. V B for 150 GPa.

Figure 2 first shows the formation enthalpies of the hydrides at 29 GPa (top panel). At this pressure, none of the hydrides beyond MnH is stable. However, the enthalpies of three hydrides from the series have clearly started to drop: MnH_2, MnH_3, and MnH_7. We see that at 29 GPa, MnH_2 is very close from the convex hull, and indeed, a few GPa beyond, this manganese dihydride is the first compound containing more hydrogen than MnH that becomes stable. MnH_2 is followed by MnH_7, which becomes stable at ∼44 GPa (surprisingly, the enthalpy of MnH_7 drops more quickly with increasing pressure than that of MnH_3). At 44 and 58 GPa, the two hydrides MnH_2 and MnH_7 lie on the convex hull.

The structure found for MnH_2 is the same as that observed in several transition-metal dihydrides (e.g., FeH_2 and CoH_2). It is a body-centered tetragonal structure with space group $I4/mmm$. The structure of MnH_7 is hexagonal (space group P_6/mmm). It is characterized by hexagonal cages of atomic hydrogen bonded to Mn atoms, surrounding H_2 molecules. Hydrogen is thus only partially reduced into hydrides in MnH_7, a part of it remaining under the molecular form (mixed hydride).

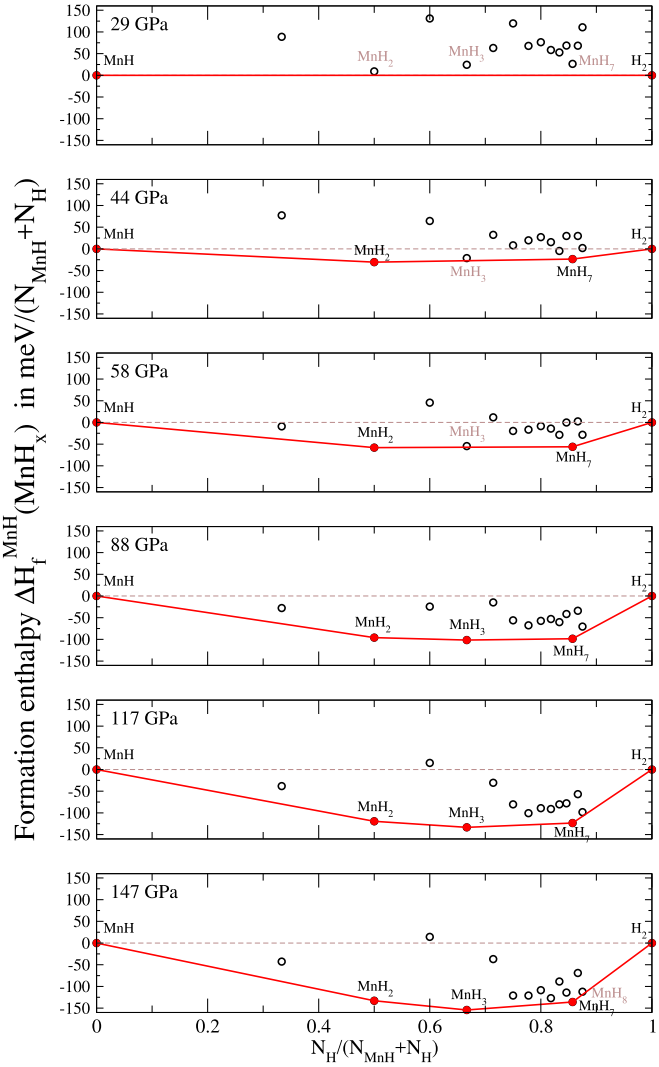

FIG. 2. Formation enthalpies of the Mn hydrides with respect to ϵ-MnH and solid hydrogen, from 29 to 147 GPa. Phonon ZPEs are not included.

Between MnH_2 and MnH_7, we find no stable structure at 44 and 58 GPa. Note that MnH_3, although not on the convex hull at 58 GPa, is rather close to it, and its formation enthalpy is decreasing with increasing pressure. At 88 GPa, MnH_3 is, indeed, now energetically stable, while MnH_7 also remains extremely stable. The structure of MnH_3 is body-centered tetragonal (space group $I4/m$) and contains 4 f.u. per primitive cell. Then, up to 147 GPa, MnH_2, MnH_3, and MnH_7 are the only compounds to be found on the convex hull beyond MnH, and MnH_7 is found as the most stable stoichiometry in hydrogen excess (the last hydride observed on the convex hull).

We also note that, at 147 GPa, MnH_8 almost lies on the convex hull. Considering how the enthalpy of this compound evolves with increasing pressure, it is highly probable that MnH_8 becomes stable for pressures beyond 150 GPa. Interestingly, the structure of this hydride contains one H_2 molecule per 2 f.u. (H-H distance = 0.73 Å within the molecule), just like that of MnH_7. We see hereafter that MnH_8 is in fact stabilized by nuclear quantum effects at 150 GPa.

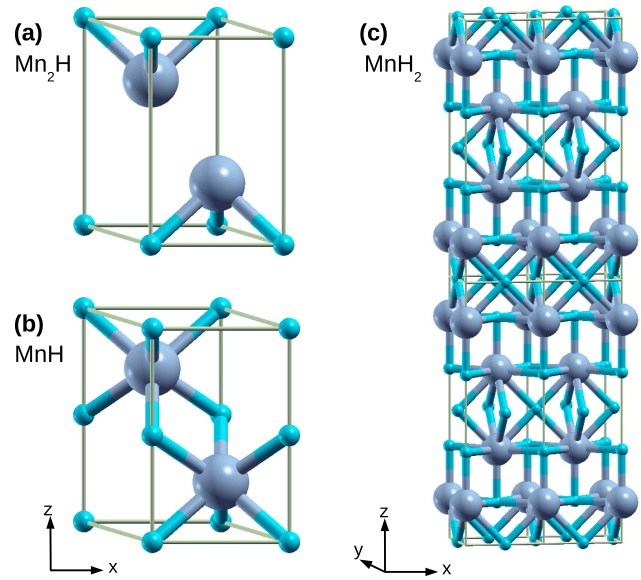

FIG. 3. Crystal structure of (a) Mn_2H (space group $P\bar{3}m1$, anti-CdI_2 type), (b) ϵ-MnH (space group $P6_3/mmc$), and (c) MnH_2 (space group $I4/mmm$). The thin solid lines materialize the primitive cell for Mn_2H and MnH, the conventional unit cell for MnH_2 (multiplicity 2).

V. PROPERTIES OF MANGANESE HYDRIDES AND SUPERHYDRIDES

A. Crystal structures

Mn_2H, ϵ-MnH, and MnH_2 crystallize in structures already encountered in other hydrides. Mn_2H and ϵ-MnH can be described as interstitial hydrides: starting from a hypothetical hcp Mn arrangement, Mn_2H is obtained by filling with hydrogen atoms half of the (0001) planes of octahedral sites, resulting in a $P\bar{3}m1$ space group. This structure is also called anti-CdI_2 type [44]; it is also reported in Cu_2H [29]. The ϵ structure of MnH is obtained by filling all the interstitial octahedral sites with H. The two structures are shown in Figs. 3(a) and 3(b).

The body-centered tetragonal structure of MnH_2 is the same as that of FeH_2 [6], CoH_2 [24] (at high pressure), and NiH_2 [25]: it consists of cubiclike MnH_3 (the arrangement observed in FeH_3 or CoH_3) slabs stacked onto each other, with two consecutive slabs being shifted in plane by (1/2, 1/2, 0) lattice vectors of the conventional cell, which yields the body-centered symmetry [Fig. 3(c)].

The body-centered tetragonal structure of MnH_3 (space group $I4/m$), in contrast, does not correspond to a structure encountered in other 3d transition-metal hydrides, to the best of our knowledge: the Mn atoms form a complex sublattice that consists in the alternance of two identical planes in which the Mn atoms are arranged in squares connected by their corners. These planes are shifted in plane with respect to each other, by (1/2,1/2,0) lattice vectors of the conventional unit cell, providing a body-centered tetragonal structure. The H atoms in MnH_3 occupy interstitial sites and belong to two subgroups that correspond to Wyckoff positions 16i or 8h (Table II). At 150 GPa, the H atoms in positions 16i have two Mn nearest neighbors at 1.57 and 1.62 Å, and two other

TABLE II. Wyckoff positions, lattice constants, and angles of the manganese hydrides found stable below 150 GPa. MnH_4 and MnH_8, given at the bottom of the table, are stabilized by nuclear quantum effects.

Compound	Space group	Pressure	Lattice constants (Å) and angles (deg)	Atom	Wyckoff position	x	y	z
Mn_2H	$P\bar{3}m1$	50 GPa	$a=b=2.4509, c=3.9095$	Mn	2d	0.33333	0.66667	0.73411
			$\alpha=\beta=90, \gamma=120$	H	1a	0	0	0
MnH	$P6_3/mmc$	150 GPa	$a=b=2.3848, c=3.7761$	Mn	2d	0.33333	0.66667	0.75
			$\alpha=\beta=90, \gamma=120$	H	2a	0	0	0
MnH_2	$I4/mmm$	150 GPa	$a=b=2.3782, c=7.8694$	Mn	4e	0	0	0.84829
			$\alpha=\beta=\gamma=90$	H	4c	0	0.5	0
				H	4e	0	0	0.64781
MnH_3	$I4/m$	150 GPa	$a=b=5.4981, c=3.4137$	Mn	8h	0.59863	0.79892	0
			$\alpha=\beta=\gamma=90$	H	16i	0.08010	0.84326	0.21136
				H	8h	0.66512	0.08765	0
MnH_7	$P6/mmm$	150 GPa	a=b=4.4262, c=2.4310	Mn	2c	0.33333	0.66667	0
			$\alpha=\beta=90, \gamma=120$	H	2e	0	0	0.35005
				H	6m	0.21084	0.42169	0.5
				H	6j	0.70360	0	0
MnH_4	$R32$	150 GPa	$a=b=4.9849, c=6.1041$	Mn	9d	0.49912	0	0
			$\alpha=\beta=90, \gamma=120$	H	18f	0.51822	0.47528	0.26076
				H	9e	0.49023	0	0.5
				H	6c	0	0	0.78214
				H	3b	0	0	0.5
MnH_8	$P\bar{1}$	150 GPa	$a=2.4409, b=4.8795, c=7.7099$	Mn	2i	0.85233	0.18657	0.72787
			$\alpha=99.89, \beta=97.98, \gamma=90.71$	Mn	2i	0.14462	0.31376	0.27329
				H	2i	0.03228	0.03451	0.14232
				H	2i	0.84902	0.39514	0.59780
				H	2i	0.39980	0.55217	0.01262
				H	2i	0.58944	0.08671	0.26812
				H	2i	0.74039	0.14104	0.52964
				H	2i	−0.03365	0.24839	−0.07428
				H	2i	0.42004	0.19375	0.85759
				H	2i	0.69081	0.87286	0.40232
				H	2i	−0.02140	0.46941	0.85723
				H	2i	0.14503	0.10424	0.40225
				H	2i	0.61053	0.05102	−0.00057
				H	2i	0.57369	0.30339	0.14135
				H	2i	0.30843	0.62603	0.59705
				H	2i	0.41054	0.41494	0.73201
				H	2i	0.25468	0.35725	0.47130
				H	2i	0.10737	0.25483	0.07615

Mn a little further at 1.72 Å. The H atoms in positions 8*h* are each surrounded by three Mn (at 1.58, 1.59, and 1.66 Å at 150 GPa), but are rather close to each other (1.39 and 1.46 Å), so that the nearest neighbors of these H atoms are also H atoms. They form small rectangular parallelepipeds, H_8, that look like the ones observed in uranium polyhydrides [18], at the exception that these H_8 cages are not connected to each other in MnH_3. Note that these short H-H distances are in line with those observed in other transition-metal polyhydrides, e.g., FeH_5, but remain significantly larger than those existing in the hydrides which are the best candidates as high-T_c superconductors at similar pressure (between ∼1.1 and 1.2 Å in LaH_{10} and CeH_9 [3], for instance). It is thus unlikely that true chemical bonds do exist between these hydrogen atoms. The structure of MnH_3 is shown in Fig. 4(a).

The structure of MnH_7 can be described as follows: the Mn sublattice is a stacking of planes within which the Mn atoms form a hexagonal two-dimensional (2D) lattice. The nearest-neighbor Mn atoms within the planes are bridged to each other by two H atoms; the nearest-neighbor Mn atoms between two consecutive planes are bridged to each other by three H atoms. This leaves large voids in the middle of the hexagons, which are filled by H_2 molecules (one H_2 molecule per 2 f.u.), each H_2 molecule being oriented perpendicular to these planes. The H-H distance within the molecules is 0.73 Å at ∼150 GPa, which is typical from the interatomic distance of the H_2 molecule. Thus, only six hydrogen atoms in the chemical formula MnH_7 are under the atomic form, the other one being under the molecular form, $1/2\ H_2$. The primitive cell contains 2 f.u. The structure is shown in Figs. 5(a) and 5(b).

The equation of states (volume versus pressure) of these different hydrides is shown in Ref. [27] (Fig. S10). From the volumes of Mn_2H, MnH, MnH_2, and MnH_3, we deduce the volume increment per hydrogen atom (Fig. S11), which is

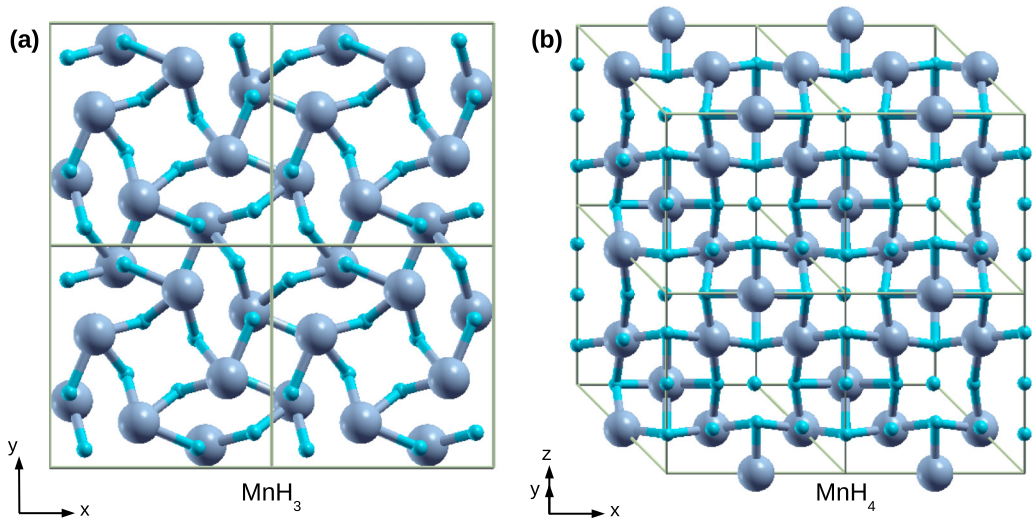

FIG. 4. Crystal structure of (a) MnH_3 (space group $I4/m$) and (b) MnH_4 (space group $R32$). The thin solid lines materialize the conventional unit cell (multiplicity 2 for MnH_3 and 3 for MnH_4).

around 1.60 $Å^3$ (resp. 1.75 $Å^3$) at 150 GPa (resp. 100 GPa). This is close to the volume expansion per H in iron hydrides [1], although a bit smaller. The Wyckoff positions, lattice constants, and angles describing these structures are given in Table II.

B. Dynamical stability and impact of phonon zero-point energies

We now question the dynamical stability of the hydrides identified as energetically stable (ϵ-MnH, MnH_2, MnH_3, and MnH_7) by computing the phonon dispersion curves within DFPT. Figure 6 displays these phonon dispersion curves, computed at 150 GPa for the four compounds, as well as the corresponding vibrational densities of states. The four hydrides are found dynamically stable at this pressure. The same calculations have also been conducted for MnH at 50 GPa, and for MnH_2 at 50 and 100 GPa (see Ref. [27], Figs. S12 and S13): these two hydrides are also found dynamically stable at those pressures.

We note that, in MnH, MnH_2, and MnH_3, the dynamics of the heavy Mn atoms and that of the light H atoms are well separated (nonoverlapping peaks in the vibrational density of states), while this is not the case in MnH_7. As

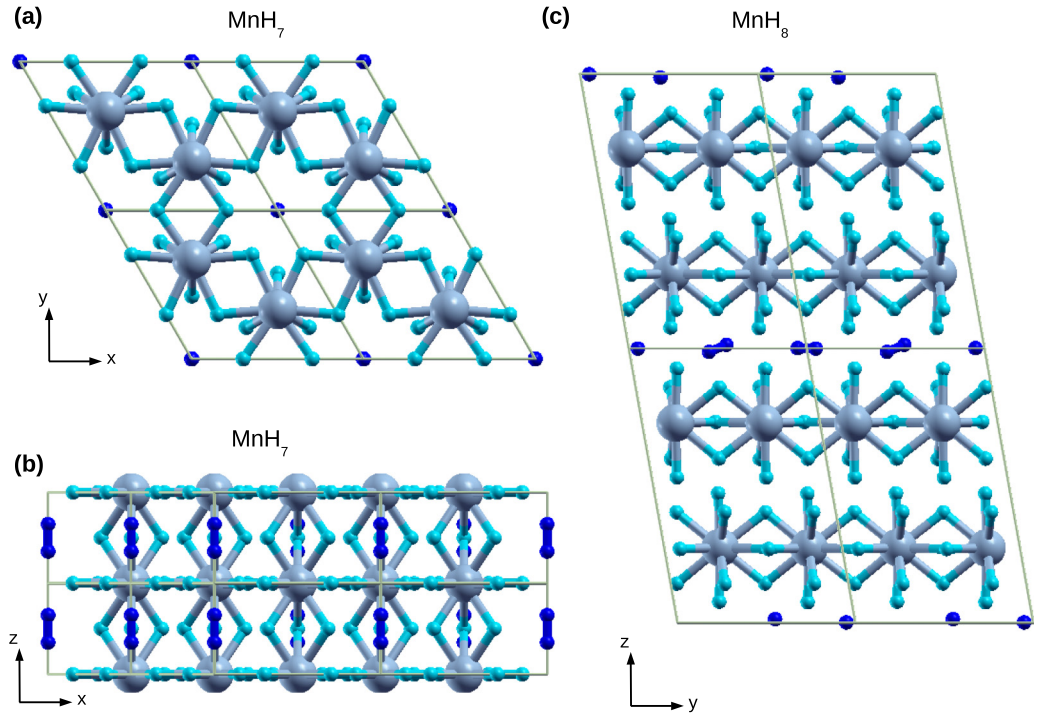

FIG. 5. Crystal structure of the mixed hydrides: (a, b) MnH_7 (space group $P6/mmm$) and (c) MnH_8 (space group $P\bar{1}$). The H_2 molecules are in dark blue, the atomic hydrogens in light blue. The thin solid lines materialize the primitive cell.

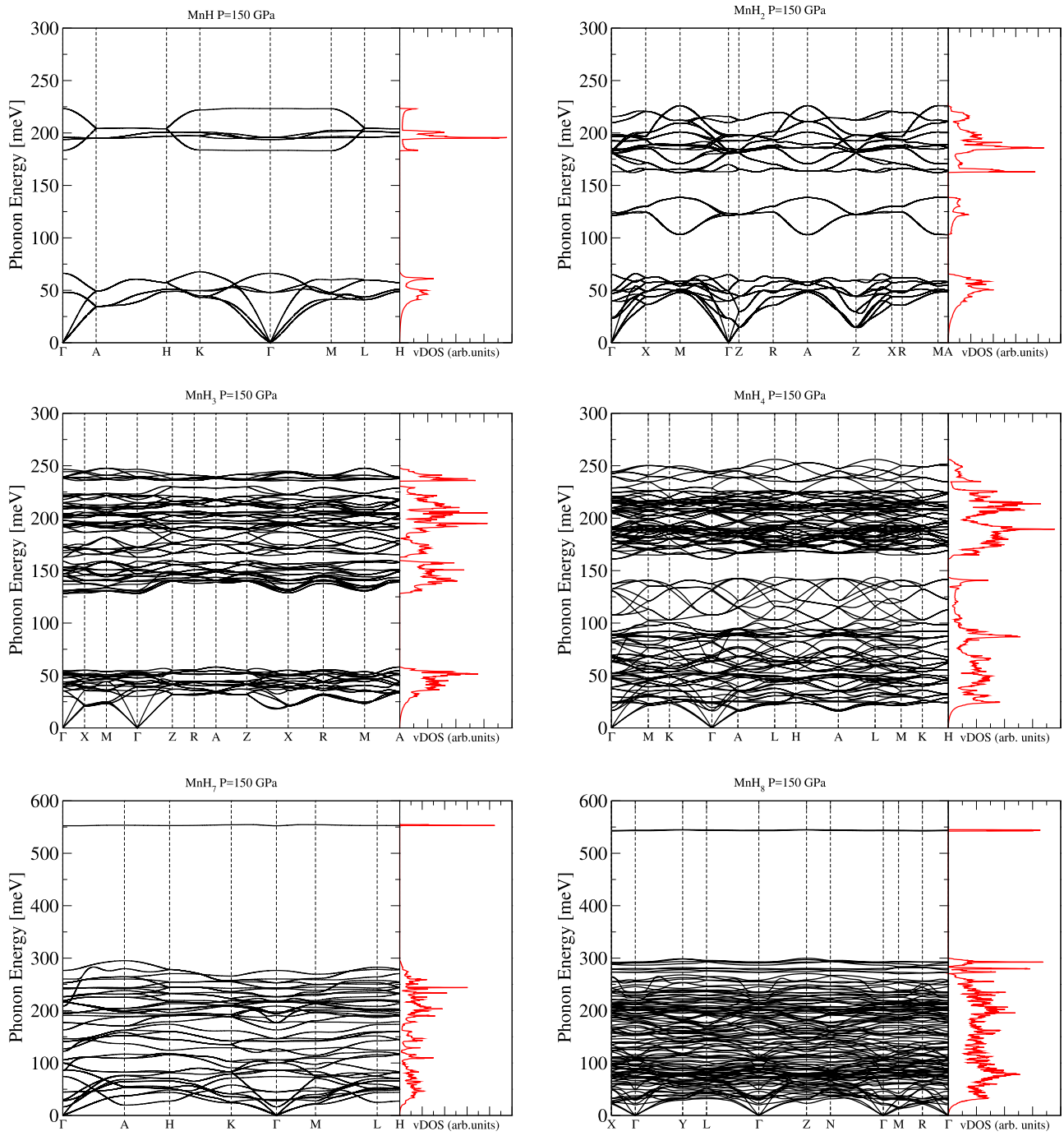

FIG. 6. Phonon band structures and vibrational densities of states for MnH, MnH_2, MnH_3, MnH_4, MnH_7, and MnH_8, computed at 150 GPa. For MnH_2 (space group $I4/mmm$) and MnH_3 (space group $I4/m$), the path in the Brillouin zone refers to the conventional (tetragonal) cell (multiplicity 2), which has been used in the DFPT calculation.

we have said, in this compound, six hydrogens per formula unit are hydrided while the latter is under the molecular form ($1/2$ H_2). The vibration modes associated with the dynamics of the six hydrogens which are under the atomic form overlap with those involving the motions of Mn. That associated with the stretching vibration of the H_2 molecule (vibron) has a very high frequency, very close to that of the vibron of free or solid molecular hydrogen ($\hbar\omega \sim 0.55$ eV).

We have also scrutinized the impact of nuclear quantum effects at 150 GPa in the harmonic approximation, by including in the formation enthalpies the contribution of phonon ZPEs. Owing to the computational cost of the DFPT calculations needed to obtain these quantities, we have limited the calculations to the structures found as being the closest to the convex hull, namely, at less than ∼30 meV. DFPT calculations were thus performed at this pressure for MnH_4, Mn_2H_9, MnH_5, Mn_2H_{11}, Mn_2H_{13}, and MnH_8 (and also solid molecular hydrogen in the $C2/c$-24 phase).

In three cases (Mn_2H_{11}, Mn_2H_{13}, and MnH_8), the phonon dispersion curves of the structures as determined by the

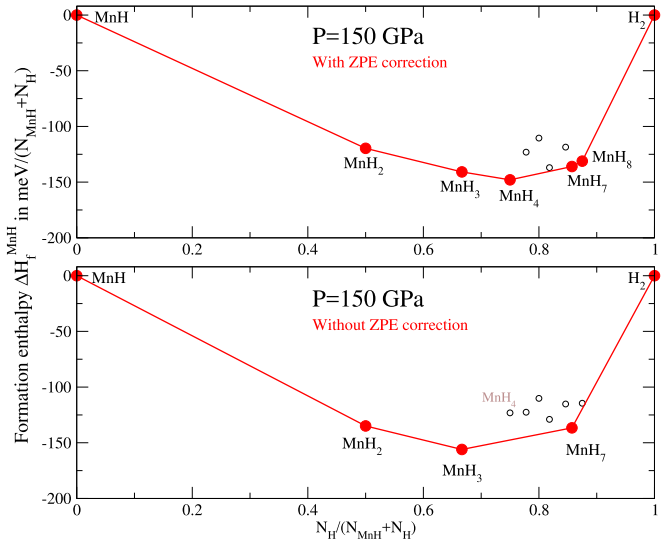

FIG. 7. Formation enthalpies of the Mn hydrides with respect to ϵ-MnH and solid hydrogen at 150 GPa, including the contribution of zero-point motions (top) and without (bottom).

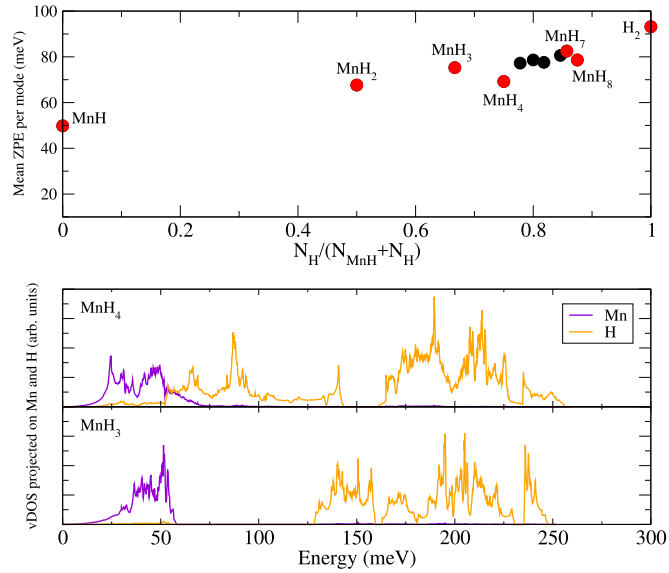

FIG. 8. Top: Zero-point energy of a formula unit divided by the number of modes (meV). Bottom: Vibrational density of states of MnH_3 and MnH_4 projected on Mn and H.

AIRSS exhibited unstable (imaginary frequency) modes. A slightly more stable structure was then obtained by displacing the atoms along these instabilities and structurally reoptimizing the system in a larger supercell. Phonons were recomputed on the final structures, which were found dynamically stable but in rather large primitive cells (26 atoms for Mn_2H_{11}, 60 atoms for Mn_2H_{13}, and 36 atoms for MnH_8). The final enthalpies are calculated using these three new structures. Note that the subsequent stabilization is weak and that the predicted stable structures before inclusion of ZPE are unchanged. More details, as well as the phonon dispersion curves of these hydrides, can be found in Ref. [27].

Figure 7 displays the formation enthalpies at 150 GPa, with and without the contribution of the ZPEs. The main impact of ZPEs is to stabilize MnH_4 and MnH_8, two phases that now lie on the convex hull at 150 GPa. Their phonon dispersion curves are shown in Fig. 6.

Note that MnH_8 was almost stable without ZPE. The structure found for MnH_8 consists of Mn monolayers within which the Mn form a 2D square lattice [Table II and Fig. 5(c)]. On both sides of each layer, the H atoms are bonded on top of Mn and in bridging positions between each pair of nearest-neighbor Mn atoms. An additional H atom also lies at the center of each square within the layer, but is placed closer to one Mn. Thus, each Mn is bonded to 11 H atoms. H_2 molecules are inserted in half of the interlayer spaces (the H-H distance in the molecule is 0.73 Å). The vibron which is the signature of the presence of molecular H_2 is clearly visible on the phonon dispersion curves at high energy (Fig. 6).

The stabilization of MnH_4 by phonon ZPEs, however, is more surprising. MnH_4 at this pressure adopts a rhombohedral structure (space group $R32$, see Table II), which can be seen as resulting from a slight distortion of a parent cubic structure (space group $Pm\bar{3}m$, 3 f.u. per primitive cell; see Table S2 in Ref. [27]). This structure possesses a few similarities with that of MnH_3 [see Fig. 4(b)]. To provide an explanation for the stability of MnH_4, we plot in Fig. 8 (top) the averaged ZPE per vibration mode as a function of hydrogen content. It can be observed that this ZPE in MnH_4 is indeed significantly smaller than in MnH_3 and in the following hydrides. This behavior may be understood from the phonon band structures (Fig. 6) and vibrational density of states (vDOS) projected on Mn and H (Fig. 8). In MnH_3, the vDOS exhibits two well-separated parts: a low-energy one ($\hbar\omega \leqslant 50$ meV) due to Mn motions, and a high-energy one ($\hbar\omega \geqslant 125$ meV) due to H motions. In MnH_4, the vibrations due to the additional H fall in the low-energy part and overlap those of Mn, giving rise to a mixed Mn-H low-energy vDOS ($\hbar\omega \leqslant 150$ meV). In other words, some H atoms in MnH_4 vibrate with eigenfrequencies which are significantly smaller than in MnH_3, which provides a smaller ZPE in MnH_4 compared to MnH_3.

Note that Mn_2H_{11} is also stabilized by phonon ZPEs, but not enough to lie on the convex hull at 150 GPa (structure given in Ref. [27]).

C. Electronic structure

The electronic band structures and electronic densities of states of MnH, MnH_2, MnH_3, and MnH_7, computed at 150 GPa, are shown in Fig. 9. As expected, MnH, MnH_2, and MnH_3 are metallic. MnH_7, however, has within the GGA-PBE approximation a very weak density of states at the Fermi level at 150 GPa, corresponding to a quasigap throughout the Brillouin zone, which is closed only around the A point. At smaller pressure, the gap in MnH_7 is open, and the compound becomes a semiconductor. At 150 GPa, still within our GGA-PBE scheme, MnH_8 is found to be a semiconductor, with a Kohn-Sham band gap of ∼0.5 eV.

D. Magnetism

α-Mn is a noncollinear antiferromagnetic (AFM) solid at ambient pressure (Néel temperature 95 K [38]). An AFM

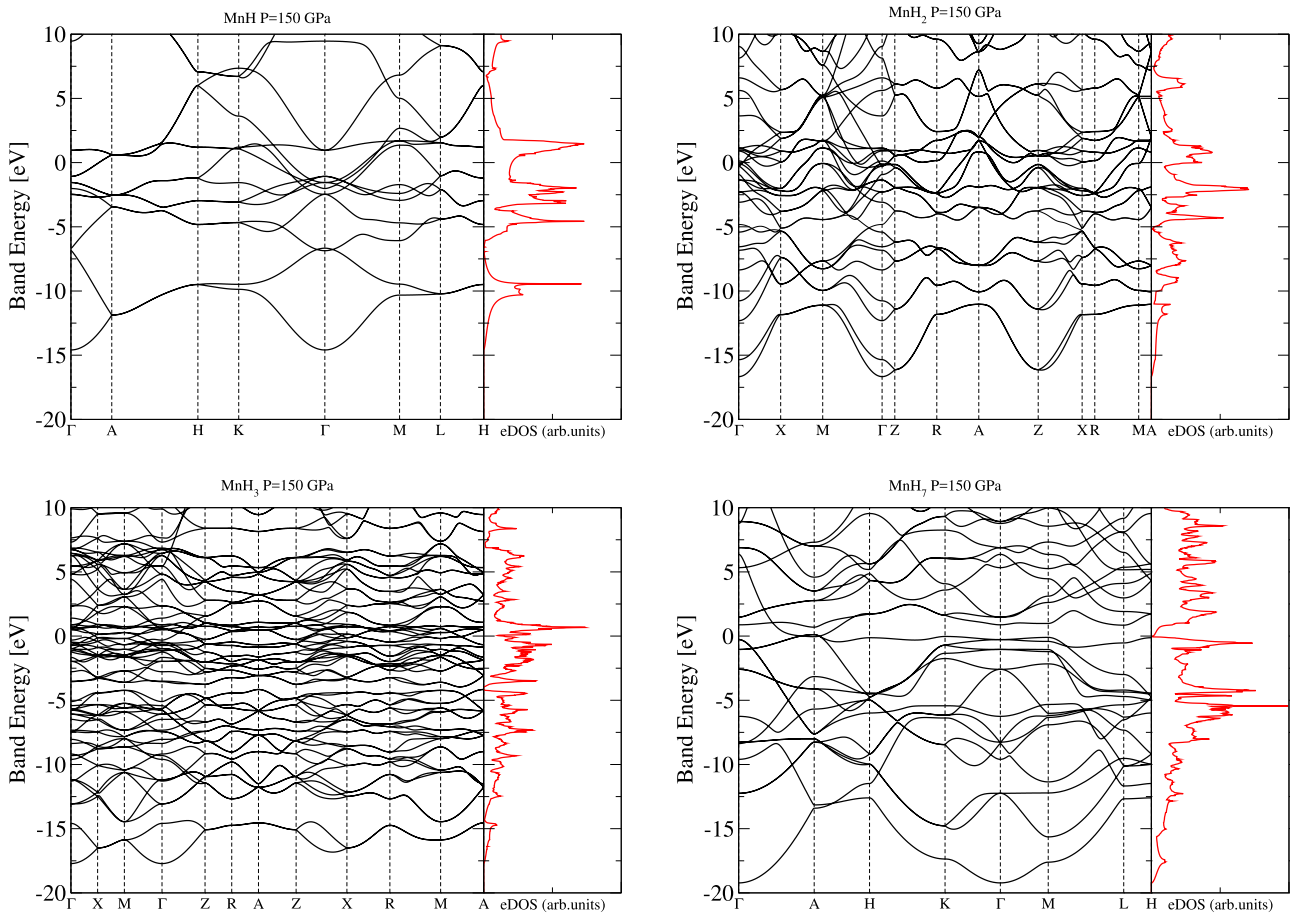

FIG. 9. Electronic band structures and electronic densities of states (eDOS) for MnH, MnH_2, MnH_3, and MnH_7 computed at 150 GPa. For MnH_2 (space group $I4/mmm$) and MnH_3 (space group $I4/m$), the path in the Brillouin zone refers to the conventional (tetragonal) cell (multiplicity 2), which has been used in the band-structure calculation. The Fermi energy is set at zero.

order is also reported (at low pressure) in ϵ-MnH_x with a Néel temperature around 360 K [44,71]: the AFM structure is due to the antiferromagnetic coupling between ferromagnetic (110) planes (of the hexagonal arrangement). This indicates that a magnetic order might exist in manganese hydrides, at least at low pressure. Also, γ-$MnH_{0.41}$ is reported as an antiferromagnet at room temperature [44,73], with a Néel temperature much above 300 K [44]. Reproducing the low-pressure AFM properties of MnH_x is, however, not the scope of the present work. It seems, nonetheless, that Mn hydrides exhibit a tendency to form rather stable magnetic structures, at least at low pressure. Here we have tested whether a ferromagnetic (FM) order can exist or not in the manganese hydrides and survive with pressure.

In Mn_2H and in ϵ-MnH, no FM order could be stabilized, regardless of the pressure, from 0 to 150 GPa.

In contrast, a weak FM order is found in MnH_2 at low pressure ($\sim 0.14\mu_B$/Mn and $0.11\mu_B$/Mn at 0 and 15 GPa), which drops to zero between 30 and 44 GPa. At 0 and 15 GPa, this FM state of MnH_2 is, however, degenerate with the nonmagnetic (NM) state (within the numerical precision of the calculation). Thus a possible FM state would not change the position of MnH_2 on Fig. 1 (it remains unstable at these low pressures).

A FM order is found stable in MnH_3 at low pressure, with magnetic moments per Mn much larger than in MnH_2. At 0 and 15 GPa, respectively, the FM state in MnH_3 is more stable than the NM state by -0.17 and -0.05 eV/f.u., and the magnetic moment is $2.02\mu_B$/Mn and $1.84\mu_B$/Mn. Like in MnH_2, this is not sufficient to stabilize MnH_3 at this pressure (see Fig. 1). Thus MnH_3 remains unstable despite FM at low pressure. Moreover, this FM state becomes rapidly less stable than the NM one above 25 GPa. It is possible to maintain it as a metastable state on a small range of pressure, up to $\sim$30 GPa. Finally, it was not possible to stabilize a FM state in MnH_7, even at low pressure.

It is unlikely that the hydrogen-rich compounds predicted in this work are high-T_c conventional superconductors. Indeed MnH_8 is found insulating and MnH_7 has a low density of states at the Fermi level. Moreover, there is no example of predicted high-T_c superconductivity in other transition-metal hydrides (excluding column IIIB of the periodic table: Sc, Y, and La), and the best candidates for high-T_c superconductivity in high-pressure hydrides remain the rare-earth hydrides and transition-metal hydrides of column IIIB.

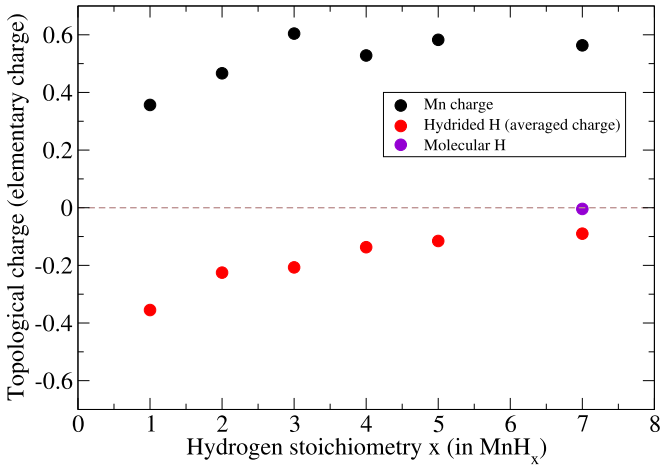

FIG. 10. Bader charge of Mn and H (in units of elementary charge) as a function of hydrogen content x in MnH_x, at 150 GPa.

E. Bader analysis of atomic charges

The atomic charges have been computed at 150 GPa, using the methodology proposed by Bader [74], for several stoichiometries, including energetically stable and unstable ones (MnH, MnH_2, MnH_3, MnH_4, MnH_5, and MnH_7). They are plotted in Fig. 10 as a function of the number of H atoms in the formula unit. The values are given in Table III for all the symmetry-inequivalent atoms. For each structure, the charge on H has been averaged over all the hydrided atoms (i.e., those that do not belong to an H_2 molecule). First of all, the Bader analysis confirms that the studied systems are hydrides, i.e., the hydrogens are *negatively* charged, and Mn is *positively* charged. There is an electron transfer from Mn to H. Second, the charge of Mn is globally increasing from MnH to MnH_3, and then saturates to a value of $\sim$+0.5–0.6, indicating that hydrogen tends to increase the oxidation process of Mn up to MnH_3. Beyond this hydride, Mn cannot release more electrons, and the released electrons are shared between the hydrogens of the structure, except when some H atoms remain molecular as in MnH_7. As a consequence, the charge of the hydrided hydrogens globally decreases to zero (in absolute value) with increasing hydrogen stoichiometry.

F. Hydrides and mixed hydrides

Up to 150 GPa, the series of the stable phases of MnH_x contains true hydrides for the lowest hydrogen content ($x \leqslant 4$), and then "mixed" compounds with hydrogen in two different states (hydride and molecular) for MnH_7 and MnH_8. One may wonder whether the large stability of MnH_7 and MnH_8 is due to the presence of molecular hydrogen in the structure; to answer that question, it is interesting to scrutinize whether the unstable compounds MnH_5, Mn_2H_{11}, MnH_6, Mn_2H_{13}, and Mn_2H_{15} also contain molecular hydrogen or not. The structures found by AIRSS for these compounds are given in Ref. [27] (Table S2). It can be seen that MnH_5, Mn_2H_{11}, and MnH_6 do not contain true molecular hydrogen (structural units H_2 with bond length 0.88 Å can be found, e.g., in MnH_6, but this does not correspond to neutral H_2 molecules). However, the unstable phases Mn_2H_{13} and Mn_2H_{15} do contain one molecular unit H_2 (see Ref. [27], Fig. S9, for the structure of Mn_2H_{13}, which is close to that of MnH_7). Thus, the presence of molecular H_2 in the structure is probably not sufficient to explain the large stability of MnH_7 and MnH_8.

The existence of such mixed compounds, containing both hydrides and H_2 molecules, is also encountered in FeH_6 [6].

VI. CONCLUSION

In this work, the AIRSS method has been used to identify the structures of manganese hydrides and superhydrides MnH_x up to $x = 8$ in the pressure range typically accessible to diamond anvil cell experiments. Upon increasing pressure, our calculations predict the successive stabilization of several hydrides, that contain more and more hydrogen: MnH, MnH_2, MnH_3, and MnH_7. At low pressure, insertion of hydrogen stabilizes an hcp arrangement of the manganese atoms, with the H atoms filling the octahedral interstitial sites of this lattice, as in Mn_2H and MnH. This is in qualitative agreement with the experiments performed on the Mn-H system up to a few tens of GPa.

The existence of manganese mono-, di-, and trihydride (MnH, MnH_2, and MnH_3) is in line with some other 3*d* transition-metal hydrides such as Fe, Co, and Cr. The structure of MnH_3, with 4 f.u. per primitive cell, however, is rather complex and differs from other known structures of transition-metal trihydrides. MnH, MnH_2, and MnH_3 are metallic compounds.

We predict the existence of a very stable MnH_7 superhydride, already present on the convex hull at $\sim$44 GPa. The crystal structure of MnH_7 contains one hydrogen molecule per 2 f.u. These H_2 molecules are aligned along hexagonal channels. At high pressure ($\sim$150 GPa) in MnH_7, the GGA-PBE provides an electronic structure with a quasigap throughout the Brillouin zone, which is closed only around one specific

TABLE III. Atomic charges (in elementary charge e) as obtained from Bader analysis for the different symmetry-inequivalent atoms in MnH, MnH_2, MnH_3, MnH_4, MnH_5, and MnH_7 at 150 GPa. The numerical error on the computation of the charge is estimated to $\sim$0.01e.

Compound Space group	MnH $P6_3/mmc$	MnH_2 $I4/mmm$	MnH_3 $I4/m$	MnH_4 $R32$	MnH_5 $C2/m$	MnH_7 $P6/mmm$
Mn	0.357 (2d)	+0.466 (4e)	+0.604 (8h)	+0.528 (9d)	+0.583 (4i)	+0.563 (2c)
H	−0.357 (2a)	−0.254 (4c)	−0.205 (16i)	−0.186 (18f)	−0.152 (8j)	−0.004 (2e)
H		−0.196 (4e)	−0.211 (8h)	−0.008 (9e)	−0.145 (4h)	−0.064 (6m)
H				−0.186 (6c)	−0.058 (4i)	−0.116 (6j)
H				−0.134 (3b)	−0.069 (4i)	

point. At 150 GPa, MnH_8 and MnH_4 are stabilized by phonon zero-point energies.

The present work should motivate experimental studies of the Mn-H system up to the high pressures accessible in diamond anvil cells.

ACKNOWLEDGMENTS

Jean-Bernard Maillet is acknowledged for his help with the generation of random structures. The XCRYSDEN software [75] has been used in Figs. 3, 4, and 5.

[1] C. M. Pépin, G. Geneste, A. Dewaele, M. Mezouar, and P. Loubeyre, Science **357**, 32 (2017).
[2] Z. M. Geballe, H. Liu, A. K. Mishra, M. Ahart, M. Somayazulu, Y. Meng, M. Baldini, and R. J. Hemley, Angew. Chem. Int. Ed. **57**, 688 (2018).
[3] N. P. Salke, M. Mahdi, D. Esfahani, Y. Zhang, I. A. Kruglov, J. Zhou, Y. Wang, E. Greenberg, V. B. Prakapenka, A. R. Oganov, and J.-F. Lin, Nat. Commun. **10**, 4453 (2019).
[4] Z. Bazhanova, A. R. Oganov, and O. Gianola, Phys. Usp. **55**, 489 (2012).
[5] C. M. Pépin, A. Dewaele, G. Geneste, P. Loubeyre, and M. Mezouar, Phys. Rev. Lett. **113**, 265504 (2014).
[6] A. G. Kvashnin, I. A. Kruglov, D. V. Semenok, and A. R. Oganov, J. Phys. Chem. C **122**, 4731 (2018).
[7] S. Zhang, J. Lin, Y. Wang, G. Yang, A. Bergara, and Y. Ma, J. Phys. Chem. C **122**, 12022 (2018).
[8] N. Zarifi, T. Bi, H. Liu, E. Zurek, J. Phys. Chem. C **122**, 24262 (2018).
[9] N. W. Ashcroft, Phys. Rev. Lett. **92**, 187002 (2004).
[10] P. Loubeyre, F. Ocelli, R. Le Toullec, Nature (London) **416**, 613 (2002).
[11] A. P. Drozdov, M. I. Eremets, I. A. Troyan, V. Ksenofontov, and S. I. Shylin, Nature (London) **525**, 73 (2015).
[12] Y. Li, J. Hao, H. Liu, J. S. Tse, Y. Wang, and Y. Ma, Sci. Rep. **5**, 9948 (2015).
[13] H. Liu, I. I. Naumov, R. Hoffmann, N. W. Ashcroft, and R. J. Hemley, Proc. Natl. Acad. Sci. USA **114**, 6990 (2017).
[14] F. Peng, Y. Sun, C. J. Pickard, R. J. Needs, Q. Wu, and Y. Ma, Phys. Rev. Lett. **119**, 107001 (2017).
[15] E. Zurek and T. Bi, J. Chem. Phys. **150**, 050901 (2019).
[16] M. Somayazulu, M. Ahart, A. K. Mishra, Z. M. Geballe, M. Baldini, Y. Meng, V. V. Struzhkin, and R. J. Hemley, Phys. Rev. Lett. **122**, 027001 (2019).
[17] A. P. Drozdov, P. P. Kong, V. S. Minkov, S. P. Besedin, M. A. Kuzovnikov, S. Mozaffari, L. Balicas, F. F. Balakirev, D. E. Graf, V. B. Prakapenka, E. Greenberg, D. A. Knyazev, M. Tkacz, and M. I. Eremets, Nature (London) **569**, 528 (2019).
[18] I. A. Kruglov, A. G. Kvashnin, A. Goncharov, A. R. Oganov, S. L. Lobanov, N. Holtgrewe, S. Jiang, V. B. Prakapenka, E. Greenberg, and A. V. Yanilkin, Sci. Adv. **4**, eaat9776 (2018).
[19] D. V. Semenok, A. G. Kvashnin, I. A. Kruglov, and A. R. Oganov, J. Phys. Chem. Lett. **9**, 1920 (2018).
[20] A. G. Kvashnin, D. V. Semenok, I. A. Kruglov, I. A. Wrona, and A. R. Oganov, ACS Appl. Mater. Interfaces **10**, 43809 (2018).
[21] T. Bi, N. Zarifi, T. Terpstra, and E. Zurek, in *Reference Module in Chemistry, Molecular Sciences and Chemical Engineering* (Elsevier, New York, 2019).
[22] S. Yu, X. Jia, G. Frapper, D. Li, A. R. Oganov, Q. Zeng, and L. Zhang, Sci. Rep. **5**, 17764(2015).
[23] L. Wang, D. Duan, H. Yu, H. Xie, X. Xiaoli, Y. Ma, F. Tian, D. Li, B. Liu, and T. Cui, Inorg. Chem. **57**, 181 (2018).
[24] M. Wang, J. Binns, M.-E. Donnelly, M. Pena-Alvarez, P. Dalladay-Simpson, and R. T. Howie, J. Chem. Phys. **148**, 144310 (2018).
[25] J. Ying, H. Liu, E. Greenberg, V. B. Prakapenka, and V. V. Struzhkin, Phys. Rev. Mater. **2**, 085409 (2018).
[26] J. Binns, M.-E. Donnelly, M. Wang, A. Hermann, E. Gregoryanz, P. Dalladay-Simpson, and R. T. Howie, Phys. Rev. B **98**, 140101(R) (2018).
[27] See Supplemental Material at http://link.aps.org/supplemental/10.1103/PhysRevB.100.224102 for more details about unstable hydrides, equations of state of stable hydrides, and pressure evolution of phonon dispersion curves.
[28] A. Marizy, G. Geneste, P. Loubeyre, B. Guigue, and G. Garbarino, Phys. Rev. B **97**, 184103 (2018).
[29] X.-H. Xiao, D.-F. Duan, Y.-B. Ma, H. Xie, H. Song, D. Li, F.-B. Tian, B.-B. Liu, H.-Y. Yu, and T. Cui, Front. Phys. **14**, 43601 (2019).
[30] X. Li and F. Peng, Inorg. Chem. **56**, 13759 (2017).
[31] R. Quijano, R. de Coss, and D. J. Singh, Phys. Rev. B **80**, 184103 (2009).
[32] X. Ye, N. Zarifi, E. Zurek, R. Hoffmann, and N. W. Ashcroft, J. Phys. Chem. C **122**, 6298 (2018).
[33] H. Sugiura, S. M. Filipek, V. Paul-Boncour, I. Marchuk, R.-S. Liu, and S. I. Pyun, Nukleonika **51**, S73 (2006).
[34] L. Pauling, J. Am. Chem. Soc. **54**, 3570 (1932).
[35] A. L. Allred, J. Inorg. Nucl. Chem. **17**, 215 (1961).
[36] V. E. Antonov, T. E. Antonova, N. A. Chirin, E. G. Ponyatovsky, M. Baier, and F. E. Wagner, Scr. Mater. **34**, 1331 (1996).
[37] H. Fujihisa and K. Takemura, Phys. Rev. B **52**, 13257 (1995).
[38] D. Hobbs, J. Hafner, and D. Spisak, Phys. Rev. B **68**, 014407 (2003).
[39] M. Krukowski and B. Baranowski, Rocz. Chem. **49**, 1183 (1975).
[40] M. Krukowski and B. Baranovski, J. Less Common Met. **49**, 385 (1976).
[41] E. G. Poniatowski and I. T. Belash, Dokl. Akad. Nauk SSSR **224**, 607 (1975).
[42] I. T. Belash, B. K. Ponomarev, V. G. Thiessen, N. S. Afonikova, V. Sh. Shekht-man, and E.G. Ponyatovsky, Fiz. Tverd. Tela **20**, 442 (1978).
[43] A. San-Martin and F. D. Manchester, J. Phase Equilib. **16**, 255 (1995).
[44] V. E. Antonov, J. Alloys Compd. **330–332**, 110 (2002).
[45] V. E. Antonov, K. Cornell, B. Dorner, V. K. Fedotov, G. Grosse, A. I. Kolesnikov, F. E. Wagner, and H. Wipf, Solid State Commun. **113**, 569 (2000).
[46] Y. Fukai and H. Ishikawa, Z. Phys. Chem. (Muenchen, Ger.) **163**, 479 (1989).

[47] S. M. Filipek, S. Majchfeak, A. B. Sawaoka, and M. Cernansky, High Pressure Res. **7**, 271 (1991).

[48] S. M. Filipek, H. Sugiura, and A. B. Sawaoka, High Pressure Res. **4**, 354 (1990).

[49] Y. Fukai, T. Haraguchi, H. Shinoniya, and K. Mori, Scr. Mater. **46**, 679 (2002).

[50] L. Morris, U. James, J. Hales, M. L. Trudeau, P. Georgiev, J. P. Embs, J. Eckert, N. Kaltsoyannis, and D. M. Antonelli, Energy Environ. Sci. **12**, 1580 (2019).

[51] C. J. Pickard and R. J. Needs, J. Phys.: Condens. Matter **23**, 053201 (2011).

[52] H. T. Stokes,D. M. Hatch, and B. J. Campbell, findsymSoftware Suite, iso.byu.edu, https://stokes.byu.edu/iso/isotropy.php.

[53] H. T. Stokes and D. M. Hatch, J. Appl. Cryst. **38**, 237 (2005).

[54] The routines for generating the random numbers have been taken from R. Chandler's homepage. See R. Chandler and P. Northrup, http://www.ucl.ac.uk/~ucakarc/work/software/randgen.txt.

[55] X. Gonze, F. Jollet, F. Abreu Araujo, D. Adams, B. Amadon, T. Applencourt, C. Audouze, J.-M. Beuken, J. Bieder, A. Bokhanchuk, E. Bousquet, F. Bruneval, D. Caliste, M. Côté, F. Dahm, F. Da Pieve, M. Delaveau, M. Di Gennaro, B. Dorado, C. Espejo, G. Geneste, L. Genovese, A. Gerossier, M. Giantomassi, Y. Gillet, D. R. Hamann, L. He, G. Jomard, J. Laflamme Janssen, S. Le Roux, A. Levitt, A. Lherbier, F. Liu, I. Lukačević, A. Martin, C. Martins, M. J. T. Oliveira, S. Poncé, Y. Pouillon, T. Rangel, G.-M. Rignanese, A. H. Romero, B. Rousseau, O. Rubel, A. A. Shukri, M. Stankovski, M. Torrent, M. J. Van Setten, B. Van Troeye, M. J. Verstraete, D. Waroquiers, J. Wiktor, B. Xu, A. Zhou, and J. W. Zwanziger, Comput. Phys. Commun. **205**, 106 (2016).

[56] P. E. Blöchl, Phys. Rev. B **50**, 17953 (1994).

[57] M. Torrent, F. Jollet, F. Bottin, G. Zérah, and X. Gonze, Comput. Mat. Sci. **42**, 337 (2008).

[58] J. P. Perdew, K. Burke, and M. Ernzerhof, Phys. Rev. Lett. **77**, 3865 (1996).

[59] F. Jollet, M. Torrent, and N. Holzwarth, Comput. Phys. Commun. **185**, 1246 (2014).

[60] H. Kitamura, S. Tsuneyuki, T. Ogitsu, and T. Miyake, Nature (London) **404**, 259 (2000).

[61] G. Geneste, M. Torrent, F. Bottin, and P. Loubeyre, Phys. Rev. Lett. **109**, 155303 (2012).

[62] M. P. Surh, K. J. Runge, T. W. Barbee, E. L. Pollock, and C. Mailhiot, Phys. Rev. B **55**, 11330 (1997).

[63] Y. Crespo, A. Laio, G. E. Santoro, and E. Tosatti, Phys. Rev. B **84**, 144119 (2011).

[64] C. J. Pickard and R. J. Needs, Nat. Phys. **3**, 473 (2007).

[65] C. Audouze, F. Jollet, M. Torrent, and X. Gonze, Phys. Rev. B **73**, 235101 (2006).

[66] C. Audouze, F. Jollet, M. Torrent, and X. Gonze, Phys. Rev. B **78**, 035105 (2008).

[67] W. L. Mao, W. Sturhahn, D. L. Heinz, H.-K. Mao, J. Shu, and R. J. Hemley, Geophys. Res. Lett. **31**, L15618 (2004); J. V. Badding, R. J. Hemley, and H.-K. Mao, Science **253**, 421 (1991).

[68] T. R. Paudel, S. S. Jaswal, and E. Y. Tsymbal, Phys. Rev. B **85**, 104409 (2012).

[69] We use the expression $2\Delta\mu_H(T, P_{H_2}) = H_0 - TS_0 + \mathcal{N}c_p(T - T_0) - Tc_p\mathcal{N}\ln(\frac{T}{T_0}) + k_b\mathcal{N}T\ln(\frac{P_{H_2}}{P^0})$, with $c_p = 3.5k_B$, $P^0 = 1$ atm, $T_0 = 298$ K, $\mathcal{N}$ is the Avogadro number, $H_0 = 8468$ J mol^{-1}, and $S_0 = 130.68$ J mol^{-1} K^{-1}, two experimental values for the standard enthalpies and entropies of the hydrogen gas, taken from Ref. [70].

[70] *CRC Handbook of Chemistry and Physics*, 85th ed., edited by D. R. Lide (CRC Press, Boca Raton, FL, 2004).

[71] A. V. Irodova, V. P. Glazkov, V. A. Somenkov, S. Sh. Shil'stein, V. E. Antonov, E. G. Pony-atovsky, Sov. Phys. Solid State **29**, 1562 (1987).

[72] S. Sh. Shilstein, V. P. Glazkov, A. V. Irodova, V. A. Somenkov, V. E. Antonov, and E. G. Ponyatovsky, Z. Phys. Chem. (Muenchen, Ger.) **146**, 129 (1985).

[73] V. K. Fedotov, V. E. Antonov, A. I. Kolesnikov, A. I. Beskrovnyi, G. Grosse, and F. E. Wagner, Solid State Commun. **107**, 787 (1998).

[74] R. W. Bader, Chem. Rev. (Washington, DC, U.S.) **91**, 893 (1991).

[75] A. Kokalj, J. Mol. Graphics Modell. **17**, 176-179 (1999), code available from http://www.xcrysden.org/.